RSC Advances

ROYAL SOCIETY OF CHEMISTRY

www.rsc.org/advances

Journal Name

ARTICLE

Nano-carbon: Preparation, Assessment, and Applications for NH_3 Gas Sensor and Electromagnetic Interference Shielding

Received 00th January 20xx,
Accepted 00th January 20xx

DOI: 10.1039/x0xx00000x

www.rsc.org/

A. D. Ugale, R. V. Jagtap, D. K. Pawar, S. S. Datar, S. N. Kale, and P. S. Alegaonkar†

We report on preparation and characterizations of nano-carbon for its applications in NH_3 sensing and electromagnetic interference shielding (EMI, X-band, 8-12 GHz). Nano-carbon was synthesized, by combustion of 1,7,7-trimethyl-bi-cycloheptan (Camphor, $C_{10}H_{16}O$) deposited at 77 K. Morphological analysis showed nano-carbon was spherically concentric shells (40-50 nm); interconnected spatially. In Raman, vibration modes observed at 1390 (D) and 1580 (G) cm^{-1}, indicated presence of sp^3 within sp^2 shells. UV-visible and photoluminescence spectroscopic analysis revealed that, band gap of nano-carbon was 4.5 eV with midgap of 2.7 eV and two flouro-excited states; making it useful for Fabry-Perot interferometer optical fibre gas sensor. Details of sensor system, its mechanism and transfer function analysis is presented. The system sensitivity was 3 ppm with response and recovery time, respectively, 5 and 8 s. The molecular imprint of NH_3 on nano-carbon (1-5 ppb C-loss/10cycles; 2:1, sp^3 : sp^2 rupture) was obtained that set life time of sensor probe. In EMI, % reflection of nano-carbon was comparable with copper. The losses due to hopping and migration current were large in nano-carbon and attributed to in-plane σ-bond and tetrahedral sites in nano-carbon that interacted with radiation at higher skin depth, around four times more than that of copper. Details of EMI shielding mechanism is presented.

A Introduction

Search for multifunctional material, especially, for gas sensing and electromagnetic interference(EMI) shielding is of great importance in military and civil domains. In recent years, nano-carbon such as carbon nanotubes, reduced graphene oxide, and graphene have become most popular sensing probes for gas detection,[1] particularly, for ammonia (NH_3). It has been reported that, nano-carbon showed good NH_3 sensitivity due to unique structure e.g., small size, large specific surface area,[2] and outstanding electronic properties such as high electron mobility,[3] sensitivity to electrical perturbations through NH_3 molecules. Hu et al. demonstrated NH_3 gas sensor based on reduced graphene oxide, at room temperature.[4] Cui et al. developed silver nanocrystal incorporated carbon nanaotubes for NH_3 sensors at room temperature.[5] Ghosh et al. found NH_3 sensitivity in the range of 200 to 2800 ppm, for reduced graphene oxide sensor probe.[6] Mao et al. reviewed sensor study, focused on challenges and opportunities of nano-carbon based materials for gas detection.[7] Further, the importance of EMI shielding has increased greatly as today's fast developing society is more dependent on electronics and growth of radio frequency radiation sources. The electromagnetic radiation, particularly, that at microwave frequencies tend to interfere with radars and electronics. Such interference is assumed to be strategically adverse in defence and, moreover, is hazardous in civil sector.[8] Cao et al. has studied temperature dependence of permittivity of ultrathin graphene composites [9] and multi-region microwave absorption of nanoneedle-like ZnO.[10] In another study, He et al. reported tuneable electromagnetic attenuation capability of magnetic nanoparticles decorated reduced graphene oxides in microwave region.[11] Wen et al. found the thinnest and most lightweight materials with highly efficient microwave attenuation performance of reduced graphene oxide.[12] In most of these studies, the emphasis is on graphene based nano-carbon material correlating dielectric, EMI shielding, and microwave-absorption performance.[13,14]

The another class of carbon is the amorphous nano-carbon, the broad name used for soot of the carbonaceous element. It is primarily composed of nano-carbon in the form of agglomerated nano-particles with diameter of about 10-50 nm. They have neither graphite nor diamond like phase of carbon[15] and lead to interesting physical properties. Their degree of sp^2 graphitic ordering ranges from nano-crystalline graphite to glassy carbon. One can define diamond like carbon as amorphous carbon which can have mixture of sp^3 and sp^2 sites with composition depending upon formation of amorphous phase. The basic element which makes this material interesting is their bond molecular environment that consists of σ and π states. They have significantly different behaviour and properties changes dramatically with composition of sp^2 and sp^3. Such nano-carbon is light weight, easy to synthesize, cost effective, stable at high temperature, and ecofriendly. The focus of the present work is to evaluate performance of such nano-carbon,

Department of Applied Physics, Defence Institute of Advance Technology, Girinagar, Pune 411025, MS, India
† Corresponding author: Prashant S. Alegaonkar (Tel.: +91-20-2430 4592, e-mail: prashantalegaonkar@dait.ac.in).
Electronic Supplementary Information (ESI) available: [details of electron microscopy images are available in supplementary information]. See DOI: 10.1039/x0xx00000x

obtained by pyrolysis of camphor at low temperature, for NH_3 gas sensing and EMI shielding applications. The fabricated nano-particles consisted of sp^2+sp^3 carbon having bond disorder in terms of unsaturated dangling bonds, vacancy mediated defects, etc. The nano-carbons were integrated with optical fibre based gas sensor. The performance characteristic of the designed sensor was investigated for full scale detection, response function and limit of detection. The evaluation of nano-carbon for EMI shielding was demonstrated by analysing dielectric function, dc and ac conductivity, skin depth and % reflection. Details are presented.

B Results and discussion

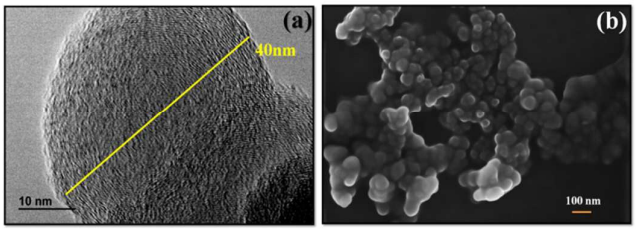

Figure 1: Recorded images (a) HRTEM and (b) FESEM of nano-carbon.

a Morphological analysis

Figure 1 shows typical (a) HRTEM and (b) FESEM image of nano-carbon. The obtained structures are spherical shaped coagulated nano-carbon. It shows nature of deposited amorphous carbon soot in the form of spheres of dimension around 40-50 nm. The HR imaging revealed that, the nano-carbon consisted of concentric shells. At several sites, shell discontinuity and formation of amorphous zone was seen. Especially, at the outermost shell, the degree of amorphization seems to be more prominent. At some sites, we have seen highly crystalline outer shells detached from the core of nano-carbon. The two regions seem to be separated by un-crystalline carbon zones. In most of the cases, crystallinity was prominently observed in nano-carbon. Though, TEM gives two dimensional imaging, it seems that nano-carbon was interconnected. The SEM results resemble with TEM findings. The coagulated and connected nano-particles were clearly visible as seen in Figure 1(b). The nano-carbon has formed three dimensional structures with homogeneous particle size distribution. A large number of HRTEM and FESEM micrographs were recorded and provided in supporting information. Further, the obtained nano-carbon was in powder form can be easily be transformed into a coating on a desired substrate. Such high surface area, spatial, homogeneous and mix phased nano-carbon structure looks to be advantageous for molecular sensing, radiation shielding, etc.

The great versatility of nano-carbon arises from the strong dependence of their physical properties on the proportion/ratio of sp^2 and sp^3 bonds. Raman spectrum fundamentally depends on ordering of sp^2 sites and indirectly on sp^3 content.

b Raman studies

Raman scattering is unique tool to probe sp^2 and sp^3 fraction. In this section, brief Raman spectroscopic analysis of nano-carbon is presented in light of morphological analysis.[16–18]

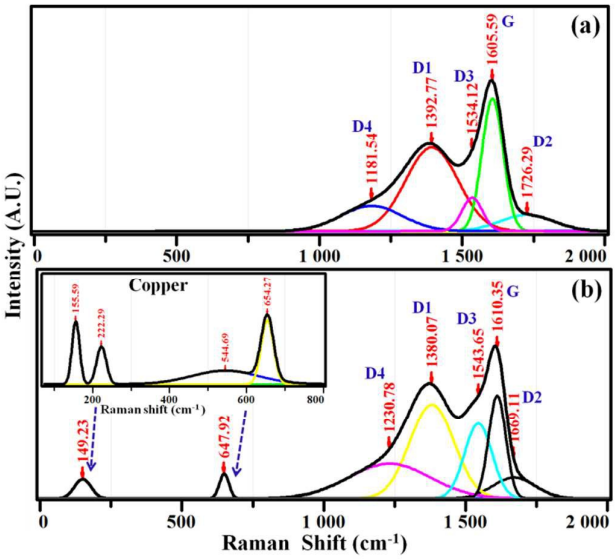

Figure 2: Recorded Raman spectra for (a) nano-carbon powder, (b) nano-carbon deposited on copper. Inset shows vibration modes of metallic copper. Arrows indicate changes in vibration modes of copper by nano-carbon.(λ ~ 457 nm).

Figure 2(a) shows recorded spectrum of free standing nano-carbon. It consisted of two peaks, D and G. Broadly, they were, respectively, assigned to sp^3 and sp^2 phases of nano-carbon. The emergence of these phases is peculiar characteristic of amorphous carbon and indicative of large disorder. To determine this, a curve fitting was carried out in terms of spectroscopic parameters such as peak position, peak width, lineshape (i.e. Gaussian, Lorentzian or a mixture of both) and band intensity. The result of this line decomposition is indicated in Figure 2. Several fits were tried leaving all spectroscopic parameters free to progress and the best fitting was invariably obtained for our spectrum. The D-peak was deconvoluted for three component namely D1 at 1392.77, D3 at 1534.12, and D4 at 1181.54 cm^{-1}. Among them, D1 and D4 were Gaussian and D3 narrow Lorentzian. The D4 is superimposed molecular vibrations of sp^2+sp^3 bonds,[19] D1 tetrahedral carbon and D3 amorphous graphitic phase. [20,21] The sp^2 carbon attached to sp^3 have vibrational features at frequencies less than 1500 cm^{-1}. Similarly, for G-band curve fitting is shown. It consisted of narrow line width feature at 1605.59 cm^{-1} (G) and broad one at 1726.2 cm^{-1} (D2) assigned to breathing mode of nano-carbon shell. The result of this fitting was in good agreement with the literature work.[22] It is interesting to note that, G mode was close to the main E_{2g2} band of crystalline graphite. This is further evidence in favour of rich sp^2 crystalline environment in nano-carbon supported by narrower line width of G compared to D-band.[19,25] Intensity of G-band was higher than that of D-band. It has dependence between the integrated intensity ratio I_D/I_G (1.5) which is inversely proportional to nano-crystalline planar size L_a ~ 3 nm.[17,23]

Figure 2(b) is Raman spectrum recorded for nano-carbon deposited on copper. The Raman finger print modes of copper ~ 200 and 500 cm^{-1} seems to be suppressed heavily while catalyzing nano-carbon. For such nano-carbon system, the I_D/I_G ratio was 2.3 with L_a ~ 2 nm. This indicated that, amount of graphitization in nano-carbon

changed when deposited on condensed copper (77 K). Perhaps L_a was incrementally enhanced in free standing nano-carbon. However, vibration modes of copper seem to be interacting with modes of nano-carbon. Interestingly, sp^3 sites have only σ states, while sp^2 sites also possess π states. They have implication on optical band structure in terms of occupancy, total energy, charge density and polarizablity to generate optically active photo-excited states.

c Optical spectroscopy: Band structure of nano-carbon

In the present work, we have demonstrated applications of the obtained nano-carbon for optical based gas sensing and EMI shielding. To utilize nano-carbon for optical applications, one need to know optical band gap and available photo-excited state of the material. UV-Visible spectroscopy along with PL provides information about band gap and excited states. Figure 3 shows recorded UV-Visible spectrum of fabricated nano-carbon in non-aqueous medium. Plot (a) shows variation in normalized absorbance (α) as a function of wavelength (in nm). It showed a sharp peak centred ~ 207 nm and a broad shoulder extended from 225-400 nm.

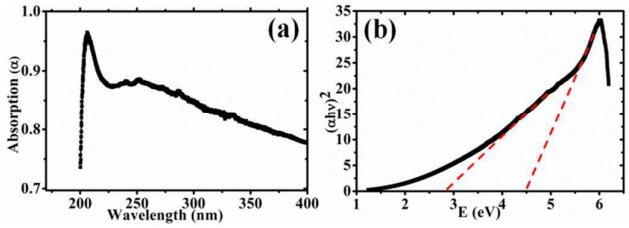

Figure 3: Recorded UV-vis absorption spectra of nano-carbon colloidal. Plot (a) absorbance (α) vs wavelength and (b) $(\alpha h\nu)^2$ vs energy. The dotted lines indicate tangent to Tauc curve.

The sharp peak was finger print of *л*-σ transition and broad feature was associated with π-π* transitions in nano-carbon. The plot (b) is Tauc graph showing $(\alpha h\nu)^2$ vs energy. The extrapolation of straight line to $(\alpha h\nu)^2 = 0$ axis gives the value of band gap.[24] The constructed tangents (red dotted lines) to the curve indicated respective optical band gap for π-σ and π-π* electronic environments. The bandgap of the nano-structure was 4.5 eV having midgap of 2.8 eV. Interestingly, the optical charge carriers have midgap state which were non-radiative in nature and having photo carrier excited states.[25]

Figure 4(a) shows PL emmision having two excited states one at 2.27 and other 1.6 eV. It showed that, nano-carbon consisted of two photo-excited states lower than midgap state. Thus, nano-carbon also possesses non-radiative fluoro-excited states. The fluoro-excited states were contributions from the dangling edges of sp^2+sp^3 hetero-structures. In nano-carbon case the lower unoccupied molecular orbital (LUMO) band consisted of both s and p orbitals, contain a total number of eight electrons per Brillion zone.[26] The band scheme is shown in Figure 4(b). By and large analysis revealed that, several states existed within HOMO-LUMO gap. These states have the wide dispersion of oscillator strength especially active in infrared and mid infrared region. This makes nano-carbon useful for optical based applications.[27]

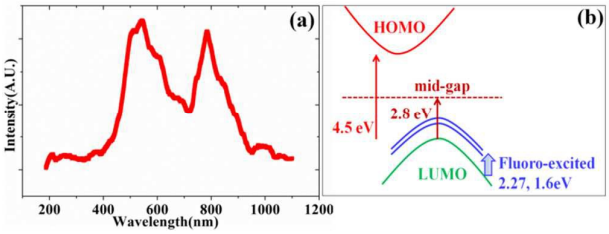

Figure 4: (a) PL spectrum recorded for nano-carbon at excitation wavelength of λ ~ 300 nm, (b) Optical band scheme of nano-carbon.

d Sensor characteristic of nano-carbon

To utility, nano-carbon specimen was deposited on optical fibre used for gas sensing application. The schematic representation of Fabry-Perot interferometer optical fibre NH_3 gas sensor is shown in Figure 5.

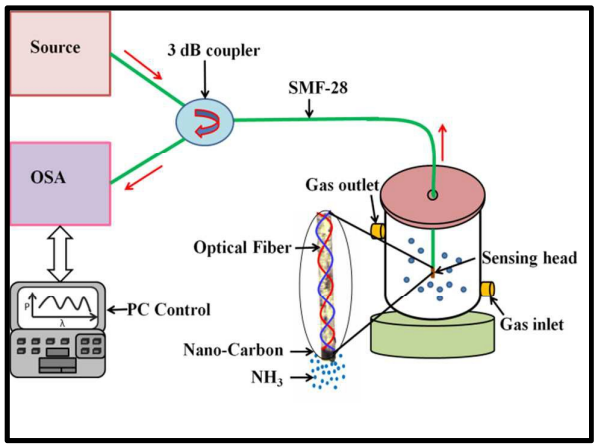

Figure 5: Elements of Fabry-Perot interferometer optical fiber gas sensor set up consisted of SMF-28, 3 dB coupler, OSA, gas sensing chamber, and PC control unit. The photograph of zoomed portion of sensor probe is shown with schematics of NH_3 molecule sensing.

In this set up, the incident mid-infrared radiation (wavelength 1510-1590 nm) from the source gets bifurcated from 3 dB coupler into the ratio of 50:50. The 50 % of light travels through SMF-28 whose one end was perfectly cleaved normal to the fibre axis. The light from the fibre end reflects back giving rise to interference pattern. Thus, the cleaved fibre end was extremely sensitive to the reflection of light. In Figure 5, zoomed portion of the fibre tip decorated with nano-carbon is shown in schematics. On interaction with NH_3 molecules, the optical band gap of the tip coating changes with change in an the interference pattern. The remaining 50 % radiation passes through OSA and was coupled to PC control unit that displayed sensing output for power and wavelength shift, as seen in Figure 6.

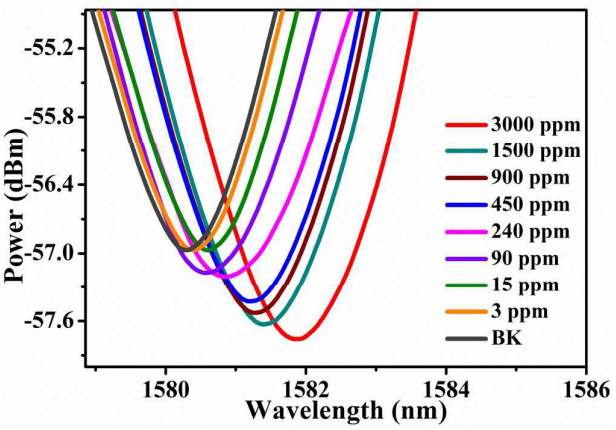

Figure 6: Sensing response of nano-carbon tip to NH_3 molecules, for a period of 180 s, at molecular concentrations ranging from 3-3000 ppm.

Initially, the spectrum was recorded for the tip in absence of NH_3. Following this, 3 ppm of NH_3 insufflate into gas chamber and onset, spectrum was recorded. The process iterated from 3-3000 ppm and at each iteration the response/recovery was monitored and recorded. It has been observed that, with subsequent increment in ppm level there was a shift in the wavelength. The sensing measurements were carried at room temperature and reliability as well as reproducibility in the sensor response has been noted well.

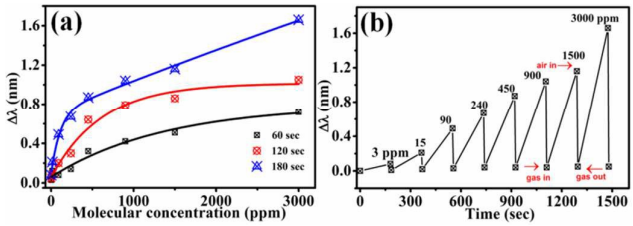

Figure 7: (a) Response function characteristics of wavelength shift (Δλ) with molar concentration (C in ppm) for different time period, and (b) Functional response of the sensor in terms of (Δλ) and time at different ppm levels.

In Figure 7(a) wavelength shift (Δλ) as function of molar concentration (C in ppm) of NH_3 is plotted for various probe/gas interaction time, 60-180 s. At 3000 ppm, the sensor showed the wavelength shift of 1.66 nm for 180 s. For 3 ppm of gas, the wavelength shift of 80 pm was observed for 180 s. It has been observed that, as the NH_3 concentration increases from 0 to 3000 ppm, the sensor showed prominent wavelength shift. All measurements were perfectly reproducible.

(i) Sensor transfer function Transfer function of a sensor system quantifies response of stimuli as a function of input. The nature of Δλ-C has been simulated for the measured time interval in the form of transfer function characteristics. At smaller time intervals i.e. upto 60 s, the function took simple form $\Delta\boldsymbol{\lambda} = \boldsymbol{K}\, \boldsymbol{e}^{\boldsymbol{C/M}}$, where, M is interaction volume, K is sensitivity constant expressed as the product of molecular interaction length and molar concentration (C). In this time domain, the simulated curve parameters, indicated that the change in wavelength was of the order of 0.8-1.0 nm affecting 1000-1500 carbon molecules. The sensitivity for molecular NH_3 was ~ 7-8 atomic distances of carbon. For higher temporal domain, the statistical interaction scenario between NH_3/nano-carbon system became more complex. This was particularly due to other physical component that started dominating the interaction such as diffusion of NH_3 in sub-surface region of individual nano-carbon, mutual chemical potential (μ) and physisorption potential (ε) experienced by NH_3/carbon ensemble, onset, within interaction volume, mismatch in the molecular vibration, etc. More diffusivity of NH_3 increased the number of carbon atom that were participating in interaction, in this time domain, which was estimated ~ 5000-6000. This had implication on both sensitivity and molar length in which sensitivity improved marginally to 10-15 molar length. For still higher sensing time, the Δλ-C transfer function took the form: $\Delta\boldsymbol{\lambda} = \prod_{i,j=1}^{3} \boldsymbol{K}\, \boldsymbol{e}^{\boldsymbol{C/M_j}}$, in which molar interaction went in the order of 10^3-10^4 and beyond. The transfer function characteristic discussed here is, strictly, at 300 K. Any departure from this value introduces adiabatic perturbative term of higher order which has potential dependence on thermodynamics of interacting system.[28] Figure 7(b) shows variation in Δλ as function of time for both response and recovery. The empirical analysis of the curve indicated that, it was composed of linear and impulse response function which is express as,

$\Delta\boldsymbol{\lambda} = \prod_{i,j=1}^{3}\{\boldsymbol{K_i T} + \frac{\boldsymbol{K_j B}}{\boldsymbol{T^3}}[\mathbf{1} - \mathbf{exp}\frac{(\dot{\mu}\,\dot{\epsilon}^{-1} + \dot{\varepsilon}\,\dot{\mu}^{-1})}{\boldsymbol{K_j}}]\}$, where, T is interaction time, B is diffusivity (cm^2-s^{-1}) of NH_3 molecule, ε and μ, respectively, rate of change of physisorption and chemisorption potential. The response and recovery time of about 5 and 8 s were noted, respectively. Table 1 indicate performance characteristics of our sensor.

Table 1: Performance sheet of nano-carbon sensor system.

Parameters	Performance and Range
Gas selectivity	NH_3 (assessed and evaluated)
Full scale detection (instrumental)	3-3000 ppm
Pulse rise time	5 s
Rise response	Linear
Pulse decay time	8 s
Decay response	Impulse
Limit of detection (intrinsic)	1-5 ppb per 10 cycles (irreversible)
Time	0-180 s
Molar transfer function	$\Delta\lambda = \prod_{i,j=1}^{3} K\ e^{C/M_j}$
Temporal transfer function	$\Delta\lambda = \prod_{i,j=1}^{3}\{K_i T + \frac{K_j B}{T^3}[1 - \exp\frac{(\dot{\mu}\,\dot{\epsilon}^{-1} + \dot{\varepsilon}\,\dot{\mu}^{-1})}{K_j}]\}$
Temperature range	300 ± 10 K

(ii) Sensing mechanism The Nano-carbon consisted of sp^2+sp^3 phase of carbon in which sp^3 phase was distributed in-homogeneously and isotropically. At the sp^2+sp^3 interface the coordination number of carbon atom connecting two phases is in disproportionate and lead to one under coordinated electron. In

addition, there were π-π* conjugated electrons in sp^2 zone. Moreover, Raman analysis revealed vacancy mediated disorder in nano-carbon system. At the vacancy site, there was non-uniform electron sharing between three uncoordinated carbon atoms. The two charge deficient carbon played role of acceptor atoms, wherein, the third carbon as the donor. The under coordinated electrons, π-π* conjugated electrons, and vacancy sites acted as the photo-carriers that participated in optical excitation process. This results into the behaviour of nano-carbon as an n-type photoconductor. The molecular NH_3 on interaction with nano-carbon, transiently, changed the midgap, fluoro-excited gap and, consequently, optical gap. In NH_3, nitrogen that carries lone pair of electrons get attracted to the charge deficient carbon atom sites by van-der-Waal interactions. The hydrogen atom in NH_3 physically adsorb at the interface of sp^2 and sp^3. Since, NH_3/nano-carbon interaction was statistical in physico-chemical nature, depending upon the stereo-regular configuration of sp^2+sp^3, there could be possibility of complete charge transfer. This will have indentation on molecular vibrations of nano-carbon, analyzed before. Interestingly, the variations has been observed in post NH_3 sensed nano-carbon revealed by Raman spectroscopy.

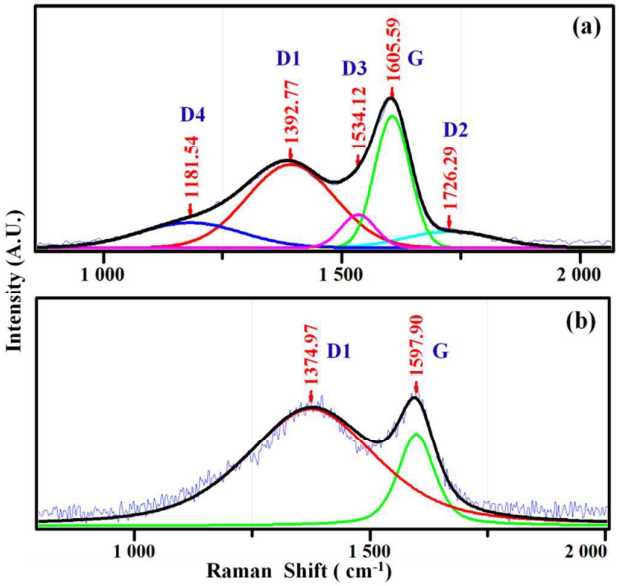

Figure 8: Recorded Raman spectrum of (a) nano-carbon decorated on optical fibre tip, (b) post NH_3 sensing (λ ~ 457 nm).

(iii) Molecular imprint of NH_3 on nano-carbon In Figure 8(b) there are significant changes in the post NH_3 treated nano-carbon sensing probe when compared to free standing nano-carbon (plot (a)). Broadly, G-band was decreased and D-band was increased and broaden. The broadening of the band indicated reduction in crystallite size of nano-carbon. Moreover, G-peak was shifted from 1605.59 to 1597.9 cm^{-1}, after NH_3 sensing. The down-shifting of G line position was attributed to enhancement in bond-angle disorder at G sites.[29] The peaks D4 and D3 were disappeared, whereas, D2 was practically vanished. This indicated that, sp^2+sp^3 sites and zones related to amorphous carbon were altered. The submerging of D3 and D4 into D1 was indicative of increased in unsaturated dangling bond character in nano-carbon. Although, the sensing action of nano-carbon probe seems to be completely reversible, macroscopically, however, at molecular level the imprint of NH_3/nano-carbon interaction is identified, clearly, by Raman spectroscopy. The sum of molecular contribution of amorphous carbon moieties i.e. D4 + D3 was of the order of 7×10^3 which got sacrificed during sensing action. Whereas, from sp^2 environment ~ 3×10^3 dangling carbon bonds were modified in sensing 3-3000 ppm of NH_3 molecules, at the end of several cycles. The rupture at sp^3 was nearly twice than at sp^2. Though the cumulative data is shown at the end of the cycles, one can investigate the effect after individual cycle. The result suggested that, the disordered carbon in nano-shell forms interstitial defects leading to molecular imprints.[22,29–31] Further, the absence of D2 showed degradation in crystallinity which form non-graphitic phase of nano-sized dimension having polycrystalline/amorphous carbon nature. This was reflected in reduction of L_a from 3 (free standing nano-carbon) to 1 nm (post NH_3 treated). The change corresponds to a second maximum in the graphite vibrational density of states near the M point of the Brillion zone boundary, which became prominent in small graphite crystallites, after NH_3 treatment. This resulted into lack of a long range translation symmetry which lead to a breakdown of the k-momentum conservation rule. [32,33]

e Nano-carbon for shield technology

Shielding of an object from incoming electromagnetic radiation is important in both military and civil sectors. EMI shielding is achieved by reflection as well as absorption of electromagnetic radiation by a material, which thereby acts as a shield against penetration of radiation.

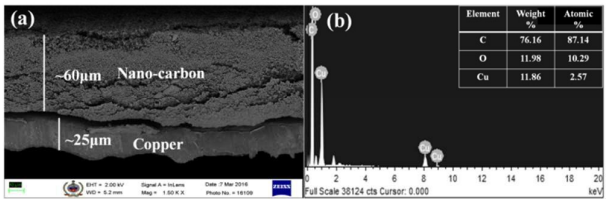

Figure 9: (a) FESEM cross-section view of nano-carbon film deposited onto copper, (b) recorded EDAX spectrum and inset in (b) shows elemental composition.

(i) Coating characteristic of nano-carbon on copper Figure 9(a) shows recorded SEM cross sectional view of nano-carbon film. The image showed thickness of nano-carbon ~ 60 µm on ~ 25 µm copper foil. The film was uniform, however, having columnar deposition inhomogeneities at certain places. In general, most of the film was continuous laterally and longitudinally. Also, at some places the peeling effect was observed. A typical micrograph is shown and others are provided in supporting information. In order to see the elemental composition of deposited nano-carbon, energy dispersive X-ray analysis (EDAX) was carried out. Figure 9(b) indicate peak associated with oxygen, carbon and copper. The inset table shows elemental composition. The high amount of oxygen ~ 12 atomic % was attributed to the presence of native oxide layer on copper.

(ii) dc Conductivity The electromagnetic rays in X-band, particularly, interact with nano-carbon material in the form of various losses such as electric conduction, hysteresis and electron spin resonance. Since, nano-carbon is nonmagnetic in nature, eddy current and electron spin resonance are dominant effect in microwave absorption. In this work, we have not carried out any study on

electron spin resonance. However, to quantify eddy current losses, electrical conductivity of nano-carbon was measured and compared with copper.

Reflection is the primary mechanism of EMI shielding which depends on conductivity, both ac and dc, of shielding material. EMI shielding depends on the interaction between mobile charge carriers (electrons or holes) of the material and the electromagnetic field. The shielding material with good electrical conductivity is necessary requirement in shield technology. Specifically, reflection loss is the function of ratio of σ_r/μ_r, where, σ_r, electrical conductivity relative to copper and, μ_r, relative magnetic permeability.[34]

Figure 10 shows measured I-V characteristic of nano-carbon compared with copper. The conductivity was estimated using: $\boldsymbol{\sigma_{dc}(S/m)} = \frac{l}{m \times h \times w}$, where, *l*, is length of active channel, *m*, slope, *h*, thickness and, *w*, width of conducting channel. Table 2 shows I-V measurement parameters estimated for both the systems.

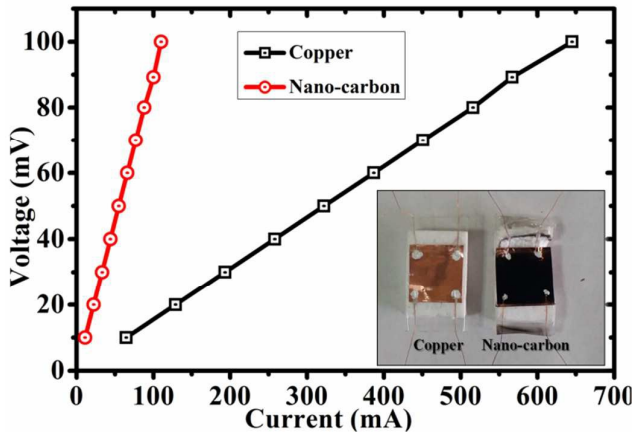

Figure 10: Measured current-voltage (I-V) characteristic of nano-carbon and copper foil. Inset shows typical photograph of samples with electrical connections and contact developed.

Table 2: I-V measurement parameters for copper and nano-carbon.

Parameters	Copper	Nano-carbon
Slope (*m*)	0.16013	0.90712
Thickness (*h*)	25 µm	60 µm
Width (*w*)	2 cm	2 cm
Length (*l*)	2 cm	2 cm
dc Conductivity (σ_{dc})	2.5×10^5 s/m	1.8×10^4 s/m
Skin depth (δ)	11 nm	42 nm

(iii) % Reflection analysis Figure 11 shows % reflection data obtained for copper and nano-carbon, in X-band regime. The amount of reflection from nano-carbon was recorded to be ~ 85%, comparable to copper (95%). For EMI shielding material, the reflection, including reflection from surface and interface scattering, will increase with increasing conductivity of the materials.

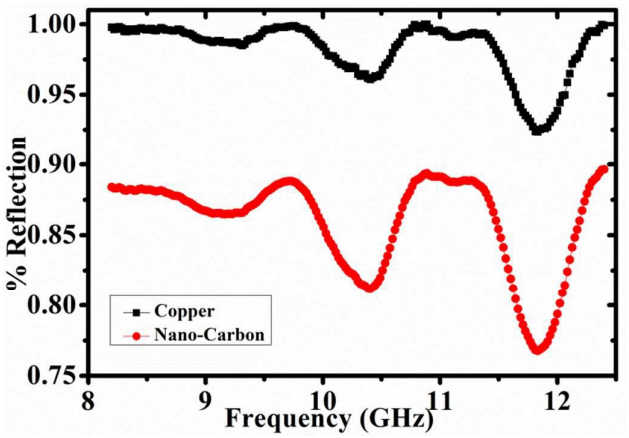

Figure 11: Recorded % Reflection for both the systems, in X-band.

Further, from Table 2, the magnitude of $\boldsymbol{\sigma_{dc}}$ for copper was ~ 10 times high compared to nano-carbon. Another important estimated parameter is skin depth, δ, the extent to which incident radiation interacted with material and given by: $\boldsymbol{\delta} = \sqrt{\frac{1}{\pi f \mu \sigma_{dc}}}$, where *f*, applied frequency, µ=1 (for copper). For 10 GHz, the value of δ was ~ 10 and ~ 40 nm for copper and nano-carbon, respectively. In both, copper and nano-carbon, reflection loss caused due to eddy current was more due to skin effect.[35,36]

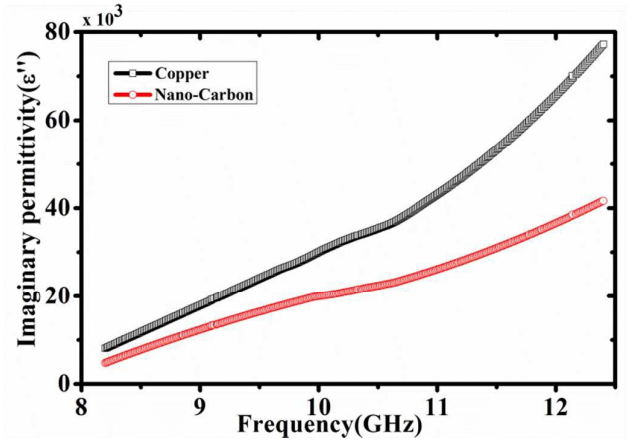

Figure 12: Recorded imaginary permittivity, ε'', as a function of frequencies, exhibiting monotonic relationship between frequency and ε''.

Figure 12 shows imaginary permittivity, ε'' of copper and nano-carbon. Reflection loss of microwave radiation is mainly due to impedance matching condition and the change of electromagnetic parameters of complex permittivity.[37] Free electrons plays important role in imaginary part of complex permittivity due to good electrical conductivity.[34,38,39] According to the free electric theory,[40] ε'' could therefore be obtained by using: $\boldsymbol{\varepsilon''} \approx \frac{\sigma_{ac}}{2\pi\epsilon_0 f}$. the relation showed that, $\boldsymbol{\sigma_{ac}}$ plays the dominating role in ε''. It seems that, the $\boldsymbol{\sigma_{ac}}$ of copper was marginally high compared to nano-carbon. This change was due to bond environment of copper and nano-carbon medium.

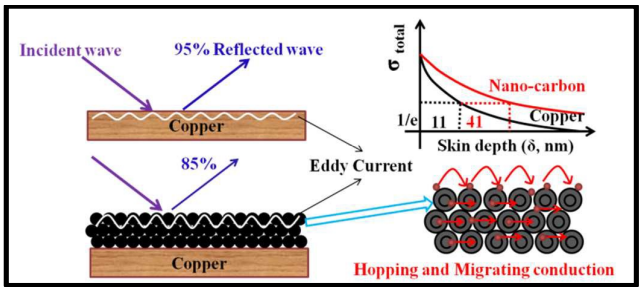

Figure 13: Schematic illustration showing electromagnetic wave interaction of nano-carbon and copper with differing skin depth level, in X-band.

(iv) Shielding mechanism The scheme of interaction mechanism of incident electromagnetic radiation with nano-carbon and copper medium is shown in Figure 13. In copper, the conduction mechanism is due to free mobile charge carriers. While in nano-carbon there exist both migrating conduction and hopping conduction due to hetero-structure sp^2+ sp^3 carbon zones.[37,41–43] Thus, increasing total conductivity in disordered spherical amorphous nano-carbon concentric shells enhances imaginary permittivity ε'' resulting in more reflection, comparable to copper. However, incident radiation of ~ 15% is attenuated within the nano-carbon layer due to larger penetration depth of electromagnetic radiation in nano-carbon compared to copper. On interaction the incident electric field component gets coupled strongly with the molecular electric field of sp^2 σ-bond. This resulted into larger dissipation of field into heat in nano-carbon.

Thus, comparative microwave reflection property of nano-carbon with copper, particularly in X band region, is advantageous. Copper being metal is high density, corrosion prone, and expensive material for shielding technology. On the other hand, nano-carbon is light in weight, ecofriendly, stable at high temperature, easy to synthesize and cost effective. Thus, nano-carbon is well suited candidate for EMI shielding over copper.

C Experimental

a Sample preparation: Low temperature nano-carbon thin film deposition

Figure 14 shows scheme of nano-carbon deposition at low temperature. The commercially available 1,7,7-trimethyl-bi-cycloheptan ($C_{10}H_{16}O$, camphor) of analytical grade was taken as the starting material to grow nano-carbon films. The deposition was carried out at 77 K under normal thermodynamic conditions. In order to deposit nano-carbon onto copper, initially, a rectangular shaped boat of dimension 5 × 3 × 1 cm^3 has been prepared from copper (thickness ~ 25 µm, purity ~ 99.8% , Alfa Aesar) and subjected to sonication. Sonication was carried out at a constant frequency of 30 kHz with power of 50 mW. The boat was immersed into methanol for cleaning and kept in water bath for a period of 15 min, for sonication at room temperature. Following this, drying process, using an IR heating lamp (power 500 W), was carried out for a period of 1 h. For deposition process, stainless steel spatula mounted on a fixed platform and prior to deposition, starting material was kept on the rectangular side of spatula. The platform was vertically moveable clamp coupled to a stand. The arrangement was such that clamp can move freely in vertical direction so that its open end can be brought in the vicinity of spatula end. This facilitates to enhance yield of nano-carbon on substrate by adjusting vertical distance between clamp and spatula mount. The boat was poured with liquid nitrogen. After camphor loading on specula, boat was clamped and brought in vicinity of precursor pellet that has been subjected to combustion for deposition. Once deposition was over, the base of boat on which thin film deposited cut into the dimensions of 2.5 × 1.5 cm^2 for assessment of deposited nano-carbon.

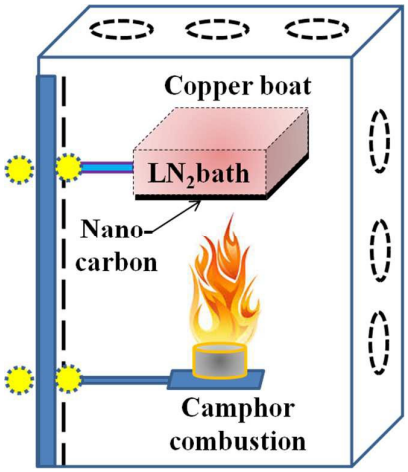

Figure 14: Scheme of nano-carbon deposition at low temperature

b Characterizations

The deposited nano-carbon specimen was gently scrubbed from the substrate using razor blade and collected into a polyethylene tetra phetelite vyal. These samples were subjected to electron microscopy, Raman, UV-visible, Photoluminescence (PL) spectroscopy.

(i) Morphological investigations using electron microscopy In order to investigate morphology of nano-carbon, high resolution transmission electron microscopy (HRTEM, G220S-Twin, Tecnai, FEI, USA) measurements were performed, using beam potential of 300 kV. For this propose, some amount of nano-carbon was immersed into Isopropyl alcohol (IPA) subjected to sonication for a period of 15-20 min. Using a micropipette, ~ 10 µl suspension was released onto a standard carbon coated copper grid. The prepared grids were allowed to dry in a closed environment. After a period of 24 h, they underwent HRTEM measurement at base pressure ~ 10^{-11} torr. A large number of images were taken in order to quantify structure, dimension and other details. In another study, surface morphology of nano-carbon was investigated using a field emission scanning electron microscopy (FESEM; Zeiss Sigma), at beam potential of 5 kV. For measurements, no gold coating was employed prior to imaging. Moreover, interface morphology of nano-carbon deposited on copper was investigated.

(ii) Raman spectroscopy Vibration spectroscopy measurements of nano-carbon, deposited nano-carbon and copper substrates were carried out using Raman spectroscopy (LABRAM HR-800). Prior to measurements, calibration of the system was carried out using silicon substrate at 457 nm excitation wavelength. The beam energy was ~ 1 mW at the sample surface. The measurements was

performed over the wavenumber range of 200-3000 cm^{-1}, at room temperature. The resolution of the system was 4 cm^{-1}. To confirm reproducibility of measured spectrum, several sites were examined for nano-carbon. For quantitative analysis, all spectra underwent several chemo-metric spectral manipulation techniques, using Labspecs 5.0 software, Horiba Industries Corporation, lesulis, France. Raleigh and florescence induced background scattering were best fitted for 4^{th} order polynomial baseline and eliminated form all spectra prior to peak fitting.

(iii) UV-visible spectroscopy For UV-visible spectroscopic measurements, nano-carbon powder was dispersed into IPA and sonicated for a period of 30 min. Following this, the suspension was immersed into spectrometer (Specord 210 PLUS, analytik jena) cuvette along with plane solution in another. The full range (200-800 nm) background spectrum was recorded and subtracted, followed by the measurements. The data of absorption (α) as function of wavelength was recorded. The absorption data was used for PL excitation.

(iv) PL spectroscopy For PL (Ocean Optics DH-2000-BAL) measurements, similar methodology was adopted as described above. The data of PL intensity as a function of wavelength (200-1200 nm) was collected for nano-carbon.

c Measurements of NH_3 gas sensing

The gas sensing set up (Photograph shown in supporting information, Figure S4) consisted of a broadband source (Micron optics, Optical Sensing Analyzer (OSA) Si720) of wavelength (1510-1590 nm, with resolution of 0.25 pm) and power of 1 mW that launches light into single mode fibre (SMF-28) through 3 dB optical coupler. The light splits at coupler in ratio of 50:50, half portion goes towards the free end of coupler and remaining light travels towards the detector. The free distal end of Y-coupler fibre was perfectly cleaved using a cleaver. The reflected light gets coupled back into the detector giving rise to interference pattern. The free end of the fibre was coated with nano-carbon.

d EMI shielding measurements

To investigate shielding performance of nano-carbon, dc conductivity (σ_{dc}), and microwave scattering measurements were performed.

(i) dc Conductivity (σ_{dc}) Using four probe technique σ_{dc} of copper and nano-carbon deposited films were determined. The data was acquired using a standard Keithley 2420 picoammeter/voltage source equipped with data acquisition software.

(ii) Microwave scattering parameters X-band (8–12 GHz, 25-37.5 mm) measurements were carried out for exploring microwave scattering properties of nano-carbon and copper. For this purpose, PNA network analyzer (Agilent, N5222A) was used having full range 10 MHz–26.5 GHz. The instrument was equipped with wave guides of dimensions 2.3 × 1.1 cm^2 for measuring S-parameters. Prior to experiments, VNA was started for 2 h for stabilizing the microwave source. Initially, full two port calibration of VNA was performed on the test specimen in order to avoid errors due to directivity, isolation, source, load match, etc. The calibration was performed in both forward and reversed direction. S11 parameter was determined from one port measured scattering data with the help of commercially available Agilent software module 85071, based on the procedure given in Agilent product note. The sample was mounted into quarterwave plate slot and measurements were performed. Set up is shown in Figure S5, in supporting information.

Conclusions

The utility of nano-carbon for effective gas sensor and efficient EMI shielding applications have been demonstrated. The nano-carbon was obtained by combustion of camphor precursor. The material was assessed for structure-property relationship using HRTEM, FESEM, Raman (λ ~ 547 nm), UV-visible, and PL spectroscopy. Morphological studies revealed that, structures were three dimensionally interconnected spherical nano-carbon. It consisted of both sp^2 and sp^3 phase in which sp^3 was inhomogeneously distributed within nano-sphere, especially, at the surface. The integrated intensity ratio I_D/I_G, estimated using Raman, was found to be 1.5 for nano-carbon. Tauc plot analysis revealed that, optical band gap of nano-carbon was ~ 4.6 eV with several photo-excited states making it useful for gas sensing application. The performance characteristics of sensor was studied, for wavelength shift with change in molecular concentration and time, at room temperature. Interaction of NH_3/nano-carbon was statistically physico-chemical in nature. The stereo-regular configuration of sp^2+sp^3 in terms of under coordinated-, π-π* conjugated-electrons, and vacancy sites made nano-carbon n-type photoconductor. On interaction, whose bandgap modifies, transiently. In Raman, contribution of sacrificed sp^3 was ~ 7×10^3, whereas, for sp^2 ~ 3×10^3 in sensing 3-3000 ppm NH_3 molecules. The rupture of sp^3 sites were twice than that of sp^2. In EMI shielding utility parameters of nano-carbon was quantified by estimating σ_{dc}, ε'', σ_{ac}' δ, and % reflection derived from S-parameters. In analysis, σ_{dc}, for nano-carbon was ten times less than copper engaging incident radiation four times higher in skin of nano-carbon. On interacting with nano-carbon, component of incident electric field got coupled strongly to sp^2 molecular field, especially, in-plane σ-bonds. Since, these were in-plane bonds, directed along carbon network, excitations of σ-electrons bridged to two carbon atoms accommodate interaction energy to dissipate within carbonaceous shells in the form of heat. The incident field was capable to rotate three atoms branched to central sp^3 carbon. As a result, overall % reflection was 85% for nano-carbon which is comparable to copper (95%). This makes nano-carbon coating useful for radar shielding material in X-band. Our result showed multifunctional character of nano-carbon obtained by facile combustion of hydrocarbon precursor.

Acknowledgements

The authors at DIAT acknowledges Dr. Surendra Pal, Vice Chancellor for support. Funding support of the ''DIAT-DRDO Programme on Nanomaterial'', DRDO is gratefully acknowledged. We are also thankful to Bhaskar Rao for helping in performing VNA measurements.

References

1 J. Kong, N. R. Franklin, C. Zhou, M. G. Chapline, S. Peng, K. Cho and H. Dai, *Science*, 2000, **287**, 622–625.

2 A. Peigney, C. Laurent, E. Flahaut, R. R. Bacsa and A.

Rousset, *Carbon N. Y.*, 2001, **39**, 507–514.
3 A. Javey, J. Guo, Q. Wang, M. Lundstrom and H. J. Dai, *Nature*, 2003, **424**, 654–657.
4 N. Hu, Z. Yang, Y. Y. Wang, L. Zhang, Y. Y. Wang, X. Huang, H. Wei, L. Wei and Y. Zhang, *Nanotechnology*, 2014, **25**, 025502.
5 S. Cui, H. Pu, G. Lu, Z. Wen, E. C. Mattson, C. Hirschmugl, M. Gajdardziska-Josifovska, M. Weinert and J. Chen, *ACS Appl. Mater. Interfaces*, 2012, **4**, 4898–4904.
6 R. Ghosh, A. Midya, S. Santra, S. K. Ray and P. K. Guha, *ACS Appl. Mater. Interfaces*, 2013, **5**, 7599–7603.
7 S. Mao, G. Lu and J. Chen, *J. Mater. Chem. A*, 2014, **2**, 5573–5579.
8 N. Li, Y. Huang, F. Du, X. He, X. Lin, H. Gao, Y. Ma, F. Li, Y. Chen and P. C. Eklund, *Nano Lett.*, 2006, **6**, 1141–1145.
9 W.-Q. Cao, X.-X. Wang, J. Yuan, W. (W. Z. . Wang and M. Cao, *J. Mater. Chem. C*, 2015, **3**, 10017–10022.
10 J. Liu, W. Q. Cao, H. B. Jin, J. Yuan, D. Q. Zhang and M. S. Cao, *J. Mater. Chem. C*, 2015, **3**, 4670–4677.
11 J.-Z. He, X.-X. Wang, Y.-L. Zhang and M.-S. Cao, *J. Mater. Chem. C*, 2016, **4**, 7130–7140.
12 B. Wen, X. X. Wang, W. Q. Cao, H. L. Shi, M. M. Lu, G. Wang, H. B. Jin, W. Z. Wang, J. Yuan and M. S. Cao, *Nanoscale*, 2014, **6**, 5754–61.
13 M. Lu, X. Wang, W. Cao and J. Yuan, *Nanotechnology*, **27**, 65702.
14 B. Wen, M. Cao, M. Lu, W. Cao, H. Shi, J. Liu, X. Wang, H. Jin, X. Fang, W. Wang and J. Yuan, *Adv. Mater.*, 2014, **26**, 3484–3489.
15 H. Darmstadt, C. Roy, S. Kaliaguine, G. Xu, M. Auger, A. Tuel and V. Ramaswamy, *Carbon N. Y.*, 2000, **38**, 1279–1287.
16 D. S. Knight and W. B. White, *J. Mater. Res.*, 1989, **4**, 385–393.
17 L. Nikiel and P. W. Jagodzinski, *Carbon N. Y.*, 1993, **31**, 1313–1317.
18 P. K. Bachmann and D. U. Wiechert, *Diam. Relat. Mater.*, 1992, **1**, 422–433.
19 B. Dippel, H. Jander and J. Heintzenberg, *Phys. Chem. Chem. Phys.*, 1999, **1**, 4707–4712.
20 L. C. Nistor, J. Van Landuyt, V. G. Ralchenko, T. V. Kononenko, E. D. Obraztsova and V. E. Strelnitsky, *Appl. Phys. A Solids Surfaces*, 1994, **58**, 137–144.
21 L. H. Robins, E. N. Farabaugh and A. Feldman, *J. Mater. Res.*, 2011, **5**, 2456–2468.
22 T. Jawhari, A. Roid and J. Casado, *Carbon N. Y.*, 1995, **33**, 1561–1565.
23 F. Tuinstra and L. Koenig, *J. Chem. Phys.*, 1970, **53**, 1126–1130.
24 J. Tauc, *Amorphous and Liquid Semiconductors*, Springer Science & Business Media, 2012, vol. 27.
25 V. L. Bonch-Bruevinch, *The Optical Properties of Solids*, Academic Press, New York and London, 1966, vol. 34.
26 J. Robertson and E. O'Reilly, *Phys. Rev. B*, 1987, **35**, 2946–2957.
27 W. A. Harrison, *Phys. Rev. B*, 1973, **8**, 4487–4498.
28 E. Llobet, *Sensors Actuators, B Chem.*, 2013, 179, 32–45.
29 R. O. Dillon, J. A. Woollam and V. Katkanant, *Phys. Rev. B*, 1984, **29**, 3482–3489.
30 J. D. Pasteris, *Appl. Spectrosc.*, 1989, **43**, 567–570.
31 J. N. Rouzaud, A. Oberlin and C. Beny-Bassez, *Thin Solid Films*, 1983, **105**, 75–96.
32 R. J. Nemanich and S. A. Solin, *Phys. Rev. B*, 1979, **20**, 392–401.
33 G. Dresselhaus, M., Dresselhaus, *Topics in applied physics: Light Scattering in Solids III*, Springer Verlag, Berlin, 1982, vol. 51.
34 Chung, D.D.L, *Carbon N. Y.*, 2001, **39**, 279–285.
35 N. Idir, Y. Weens and J. J. Franchaud, *IEEE Trans. Dielectr. Electr. Insul.*, 2009, **16**, 147–154.
36 D. X. Liu SH, Liu JM, *Electromagnetic interference shielding and microwave absorption materials*, Chemical Industrial Press, 2007.
37 M. S. Cao, W. L. Song, Z. L. Hou, B. Wen and J. Yuan, *Carbon N. Y.*, 2010, **48**, 788–796.
38 J. Wu and D. D. . Chung, *Carbon N. Y.*, 2002, **40**, 445–447.
39 B. Wen, M. S. Cao, Z. L. Hou, W. L. Song, L. Zhang, M. M. Lu, H. B. Jin, X. Y. Fang, W. Z. Wang and J. Yuan, *Carbon N. Y.*, 2013, **65**, 124–139.
40 D. T. Ramo S, Whinnery JR, *Fields and waves incommunication electronics.*, JohnWiley and Sons, New York, 1984.
41 M.-S. Cao, X.-X. Wang, W.-Q. Cao and J. Yuan, *J. Mater. Chem. C Mater. Opt. Electron. Devices*, 2015, **3**, 6589–6599.
42 M.-M. Lu, W.-Q. Cao, H.-L. Shi, X.-Y. Fang, J. Yang, Z.-L. Hou, H.-B. Jin, W.-Z. Wang, J. Yuan and M.-S. Cao, *J. Mater. Chem. A*, 2014, **2**, 10540.
43 H. Yang, M. Cao, Y. Li, H. Shi, Z. Hou, X. Fang, H. Jin, W. Wang and J. Yuan, *Adv. Opt. Mater.*, 2014, **2**, 214–219.

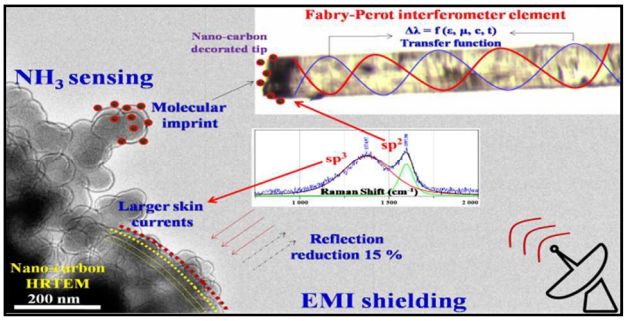

Graphical Abstract:

Performance evaluation of nano-carbon for NH_3 gas sensing and EMI shielding